Carbohydrate Polymers 117 (2015) 434–442

Contents lists available at ScienceDirect

Carbohydrate Polymers

journal homepage: www.elsevier.com/locate/carbpol

Construction of selenium nanoparticles/β-glucan composites for enhancement of the antitumor activity

Xuewei Jia, Qingye Liu, Siwei Zou, Xiaojuan Xu*, Lina Zhang

College of Chemistry and Molecular Sciences, Wuhan University, Wuchang Luojiashan, Wuhan 430072, China

ARTICLE INFO

Article history:
Received 3 April 2014
Received in revised form 5 September 2014
Accepted 25 September 2014
Available online 12 October 2014

Keywords:
Selenium nanoparticles
Triple helical lentinan
Antitumor activity

ABSTRACT

We report on a green procedure for the stabilization of selenium nanoparticles (SeNPs) by a naturally occurring β-glucan with triple helical conformation known as Lentinan (t-LNT) in water after denaturing into single chains (s-LNT) at 140 °C. The results demonstrated that the s-LNT can interact with SeNPs through Se—O—H interaction. Transmission electron microscopy (TEM), energy dispersive X-ray (EDX) spectra, UV/vis, X-ray diffraction (XRD) and dynamic light scattering (DLS) showed that s-LNT coated SeNPs to form a stable nano-composite Se/s-LNT, leading to good dispersion of SeNPs. Especially, the as-prepared Se/s-LNT composite in the solution could remain homogeneous and translucent for 30 days without any precipitates. Different size distribution of SeNPs was prepared by simply controlling the concentrations of selenite sodium and the corresponding reducing agent ascorbic acid. The size effect of SeNPs on anti-tumor activity was revealed that the SeNPs with more evenly particle size distribution show the higher anticancer activity.

1. Introduction

Selenium (Se) is not only the essential trace element for maintaining the health of mammalian animals because of its anti-oxidative and pro-oxidative effects (Bao & Williamson, 2000; Lu, Gao, & Komarneni, 2006), but also, as the active center of various enzymes in the human body, plays an important role in the disease resistance, antitumor and immunomodulating activity (Brown & Arthur, 2001; Huang, Zhang, Hou, & Chen, 2003; Zhang, Gao, Zhang, & Bao, 2001a). Se could suppress the growth of tumor cells such as prostate, lung and colorectal in several forms (Cho, Jung, & Chung, 1999; Clark et al., 1996; Fang, Han, Bi, Xiong, & Yang, 2010; Menter, Sabichi, & Lippman, 2000). But Se has a very narrow margin between its lowest acceptable levels of intake and its toxicity (Lin & Chris Wang, 2005), so we should take risk to the supplement of Se element. It has been reported that selenium nanoparticles (SeNPs) could reduce the risk of Se toxicity and be widely used in all areas of life due to its high biological activity and less toxicity tested both in vitro and in vivo, compared to the Se element (Ramamurthy et al., 2013; Wang, Zhang, & Yu, 2007; Zhang et al., 2001a; Zhang, Wang, & Xu, 2008). As an antioxidation, SeNPs can be used as a protective agent against cisplatin-induced nephrotoxicity (Li, Zhang, Xu, & Zhang, 2011a). However, the SeNPs were also prone to aggregation into large clusters in aqueous solution, leading to a lower bioactivity and bioavailability. Zhang, Wang, Bao, and Zhang (2004) observed that red SeNPs, formed in the redox system of selenite and GSH or other reducing agents, was unstable, and could further aggregate into gray and black elemental Se if there were no controlling factors (Zhang et al., 2004). Much effort has thus been devoted to developing "green" method for the feasible synthesis and dispersion of SeNPs. BSA (Zhang et al., 2004) and folic acid (FA) (Pi et al., 2013) have been reported to be used for protecting SeNPs from aggregating together. Jiang Pi et al. reported the pathway of cytotoxicity induced by FA modified SeNPs in MCF-7 cells. They found that FA-SeNPs entered into mitochondria, increased the ROS production, finally caused the damage of mitochondria and induced MCF-7 cell cycle arrest (Pi et al., 2013). Clearly, good dispersion of SeNPs will enhance the bioactivity.

As we all know, the size of nanoparticles plays an important role in their biological activity (Kashiwada, 2006; Lin & Chris Wang, 2005; Peng, Zhang, Liu, & Taylor, 2007). It has been reported that the average size of SeNPs prepared by introducing L-cysteine and *Undaria pinnatifida* polysaccharide into the water-phase redox system ranged from 59 to 220 nm (Chen, Wong, Zheng, Bai, & Huang, 2008; Li, Chen, Yang, Liu, & Zheng, 2010). Shen et al. (2008) used a polysaccharide of dextran to prepare SeNPs with average size of 36 nm through a simple method without any surfactant (Shen et al., 2008). Zhang, Wang, and Zhang (2010) also prepared SeNPs

* Corresponding author. Tel.: +86 27 68754188; fax: +86 27 68754188.
E-mail address: xuxj@whu.edu.cn (X. Xu).

http://dx.doi.org/10.1016/j.carbpol.2014.09.088
0144-8617/

with average size of 24.1 nm using a hyperbranched polysaccharide (HBP) as a stabilizer (Zhang et al., 2010). In viewing these literatures, biomolecules are a good candidate to disperse and stabilize SeNPs. In particular, polysaccharides will have potentials as a stabilizer of SeNPs because of the good water-solubility and excellent bioactivities such as anti-tumor, anti-inflammation, and so forth. But it is unfortunate that most of the authors focused on the method of synthesis and dispersion of SeNPs, and that few works on the bioactivity and the size effect of SeNPs have been reported.

Very recently, we have successfully used a β-glucan named as Lentinan (LNT) to disperse Ag (AgNPs) and Au nanoparticles (AuNPs) (Jia, Xu, & Zhang, 2013; Li et al., 2011b). LNT as a special kind of β-glucan from *Lentinus edodes*, is well known to possess significant biological and physiological activities such as in vivo anti-tumor (Sasaki & Takasuka, 1976), anti-viral (Wang et al., 2010), anti-inflammatory and immunomodulating activities (Xu, Chen, Zhang, & Ashida, 2012; Xu, Pan, Zhang, & Ashida, 2011; Xu, Yasuda, Nakamura-Tsuruta, Mizuno, & Ashida, 2012). LNT adopts β-(1,3)-D-glucan as a backbone and two β-(1,3)-Dlinked glucoses as side groups every five β-(1,3)-D-glucoside (Xu et al., 2012a), and it takes the triple-helical structure in water (denoted as t-LNT) and a single chain in dimethylsulfoxide (DMSO) or high temperature treatment (140 °C) in water (denoted as s-LNT) (Liu, Xu, & Zhang, 2012; Wang, Xu, & Zhang, 2008; Wang, Zhang, Xu, & Zhang, 2012; Xu, Wang, Cai, & Zhang, 2010). The s-LNT chains can be renatured into the triple helix (r-LNT) upon changing the DMSO content or dropping the temperature to achieve suitable conditions (Liu et al., 2012; Wang et al., 2008; Xu et al., 2010). The guests such as AuNPs can be entrapped into the reformed helical center of s-LNT with an adjustable size due to the specific character of denaturation–ranaturation for LNT in water (Jia et al., 2013). Additionally, s-LNT could interact with the DNA of poly (dA) to form a new triple helix, and was demonstrated to be used as a gene carrier (Liu, Wang, Cao, Xu, & Zhang, 2013). All our previous results indicate that LNT has strong affinity with guests including nanoparticles and DNA. Therefore, LNT will possibly be a good candidate to disperse and stabilize SeNPs. In this work, we thus used LNT to disperse and stabilize SeNPs with different size for enhancement of the bioavailability and bioactivity of elemental Se. This work will therefore provide an alternative method of stabilization of SeNPs and demonstrate the size effect of SeNPs on its antitumor activity.

2. Experimental

2.1. Materials

Na_2SeO_3 and ascorbic acid was purchased from Shanghai Chemical Reagent and used without any additional purification. Lentinan (LNT), one branched β-(1,3)-D-glucan, was isolated from the fruiting bodies of *Lentinus edodes* by extraction with 1.25 M NaOH/0.05% $NaBH_4$. The detailed procedures have previously been reported (Zhang et al., 2001b). As described in the Introduction, LNT occurs as a triple helical chain in water and so it was herein coded as t-LNT. The weight-average molecular weight (M_w) of t-LNT was determined as 8.0×10^5 by laser light scattering. Deionized water (Millipore) was utilized in all of the following experiments.

2.2. Preparation of a single chain of t-LNT

The sample t-LNT was dissolved in the deionized water and then heated at 140 °C for half an hour to break the intra- and intermolecular hydrogen bonds supporting the triple helical structure. A single chain of t-LNT (coded as s-LNT) was thus obtained in accordance with our previous work (Wang et al., 2008). It was immediately used in the subsequent experiments.

2.3. Preparation of SeNPs

SeNPs was prepared following by the procedure described by Li et al. (2011b). In brief, the aforementioned freshly prepared s-LNT (2 mg/mL) aqueous solution (20 mL) was stirred continuously in a temperature-controlled bath of 25 °C, and it was then mixed with 500 μL selenite sodium (0.1 M) and stirred for 1 min. 1 mL of aqueous ascorbic acid solution (0.2 M) was added dropwise into the resulting mixture, and it was stirred for 24 h at room temperature. The reacted product was dialyzed by using regenerated cellulose tubes (M_w cutoff 8000) against ultrapure water for 2 days. The finally resulting solution was freeze-dried with a lyophilizer (Christ Alpha 1–2, Osterode am Harz, Germany) to obtain the Selenium nanoparticle (SeNPs)/s-LNT composites (red powder), coded as Se/s-LNT.

Three Se/s-LNT composites with different particle size distribution were prepared as described above. In brief, different volumes of sodium selenite solution (0.1 M, 1 mL, 500 μL and 200 μL) and the corresponding reducing agent ascorbic acid (0.2 M, 2 mL, 1 mL and 400 μL) with the fixed ratio of sodium selenite and ascorbic acid (1:2) were added into s-LNT (2 mg/mL) aqueous solution (20 mL). Three kinds of complexes were labeled in order as Se/s-LNT-1, Se/s-LNT-2, Se/s-LNT-3.

2.4. Characterization

The morphology of the dilute solution of Se/LNT nanocomposites was observed by transmission electron microscopy (TEM, JEM-2010HT) and high-resolution transmission electron microscopy (HRTEM, JEM-2010FEF) operating at 200 kV. Samples for TEM observation were obtained by dropping the reaction solutions of 2 μL without dialysis onto carbon-coated copper grids without any purification or inspissation. A filter paper was used for rapid removal of the liquid. The reaction solution was dispersed onto a V3 TEM grid with a holey carbon support film to obtain the energy dispersive X-ray (EDX) spectroscopy.

Fourier-transform infrared spectra (FT-IR) of the samples were recorded on a Nicolet 170SX FT-IR (Spectrum One, Perkin-Elmer Co.) spectrometer in the range 4000–400 cm^{-1} using the KBr-disk method.

A UV–vis spectrophotometer (Perkin-Elmer Lambda Bio 40 UV/VIS spectrometer, USA) with 800 μL cells was used to measure the ultraviolet absorbance of SeNPs, Se/t-LNT, Se/s-LNT and t-LNT in solution at room temperature.

Wide angle X-ray diffraction (WAXD) measurements of SeNPs, Se/t-LNT, Se/s-LNT and t-LNT were carried out on a WAXD diffractometer (D8-Advance, Bruker, USA). The patterns with Cu $K\alpha$ radiation ($\lambda = 0.15406$ nm) at 40 kV and 30 mA were recorded in the region of 2θ from 5 to 70°.

Intrinsic viscosities ($[\eta]$) of the lentinan solutions were measured at 25 °C by using an Ubbelohde capillary viscometer. The kinetic energy correction was assumed to be negligible.

In all of the light scattering measurements, an ALV/DLS/SLS-5000E light scattering goniometer (ALV/CGS-8F, ALV, Germany) with vertically polarized incident light of wavelength 632.8 nm from a He-Ne laser equipped with an ALV/LSE-5003 light scattering electronics, and a multiple tau digital correlator was used to measure the molecular weight and the size of Se/s-LNT nanocomposites. All the dilute solutions were prepared by mixing the required amounts of the samples and ultrapure water in a flask by stirring gently at room temperature over night. All of the dilute solutions were finally filtered directly into the cylindrical light-scattering cuvettes using 0.22 μm pore size syringe filters (PTFE, Whatman, Inc., England).

Zeta potential measurements of three complexes were measured using a Nano-ZS ZEN3600 (Malvern Instruments, UK) at 25 °C.

The complexes were prepared by adding obtained three kinds of Se/s-LNT complexes into water solution with a storage time of 1 day at ambient temperature.

2.5. Cell culture

The human cervix carcinoma (HeLa) cells (ATCC, Rockville, MD) were kept in Dulbecco's Modified Eagle's Medium (DMEM, 4.0 g/L glucose) supplemented with 10% FBS, penicillin (100 U/mL) and streptomycin (100 μg/mL). Subculturing was done by dislodging the cells with trypsin (0.25%) and 2Na (EDTA·2Na·$2H_2O$) (0.02%), followed by centrifugation and seeding into the culture flask or plate, which was incubated at 37 °C under a humidified atmosphere of 95% air and 5% CO_2.

2.6. MTT assay

The cytotoxicities of Se/s-LNT and t-LNT were evaluated by MTT assay. Briefly, the HeLa cells were seeded in a 96-well plate at a density of 6000 cells per well, and incubated in 100 μL DMEM containing 10% FBS for 24 h. After the medium had been replace with 200 μL fresh medium, the Se/s-LNT was added and incubated for 48 h. The medium was then discarded, and 200 μL fresh DMEM and 20 μL MTT (5 mg/mL) agents were added to each well. After further incubation for 4 h, the medium was replaced with 150 μL DMSO. The absorbance was measured at a wavelength of 570 nm using a microplate reader (Bio-Rad, Model 550, USA) to determine cell viability as follows:

$$\text{cell viability}\,(\%) = \frac{\left(\text{OD}_{\text{samples}} - \text{OD}_{\text{DMSO}}\right)}{\left(\text{OD}_{\text{control}} - \text{OD}_{\text{DMSO}}\right)} \times 100$$

herein, $\text{OD}_{\text{samples}}$ and $\text{OD}_{\text{control}}$ were obtained in the presence and absence of the complex, respectively.

2.7. Measurement of ROS generation

Intracellular ROS accumulation was evaluated by DCF fluorescence assay. Briefly, cells were centrifugation at 600 × *g*, washed twice with PBS and then suspended in PBS (1×10^6 cells/mL) containing 10 μM DCFH-DA. Cells were incubated for 30 min at 37 °C as described by the manufacturer. Then, the stained cells were collected and resuspended in PBS. 20,000 cells were analyzed by flow cytometer with excitation wavelength of 488 nm and emission wavelengths of 529 nm, respectively.

3. Results and discussion

3.1. Formation of SeNPs

In the preparation of Se, with an excess of the reducing agent of ascorbic acid, the color of the reaction solution slowly turned from achromatic color to yellow, and finally turned into orange-red indicating that redox reaction occurred in the solution.

To confirm the SeNPs generated in the solution, the reaction solution was added dropwise and dried on a copper grid for TEM and EDX observation after reaction for 5 h. Fig. 1 shows the TEM image and the size distribution of the reduced Se. Clearly, Se was uniformly dispersed as SeNPs with spherical shape (Fig. 1a). Through counting 200 particles, the mean diameter of SeNPs was estimated to be ca. 28 nm. The HRTEM image of SeNPs (Fig. 1c) clearly shows the selenium crystal lattice fringes and fringe spacing, and the corresponding EDX (Fig. 1d) proved that these nanoparticles were made up of Se element. All the above results

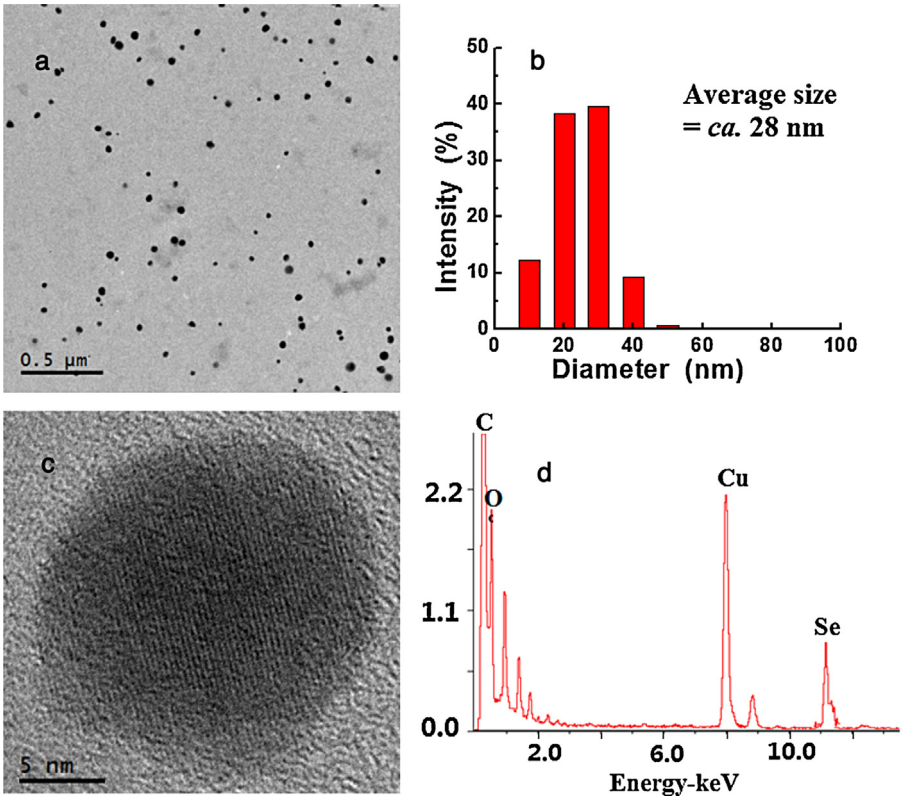

Fig. 1. (a) TEM image of SeNPs in the s-LNT aqueous solution. (b) Size distribution of SeNPs. (c) HRTEM image of an individual Se nanoparticle. (d) EDX spectrum of Se/s-LNT from HRTEM.

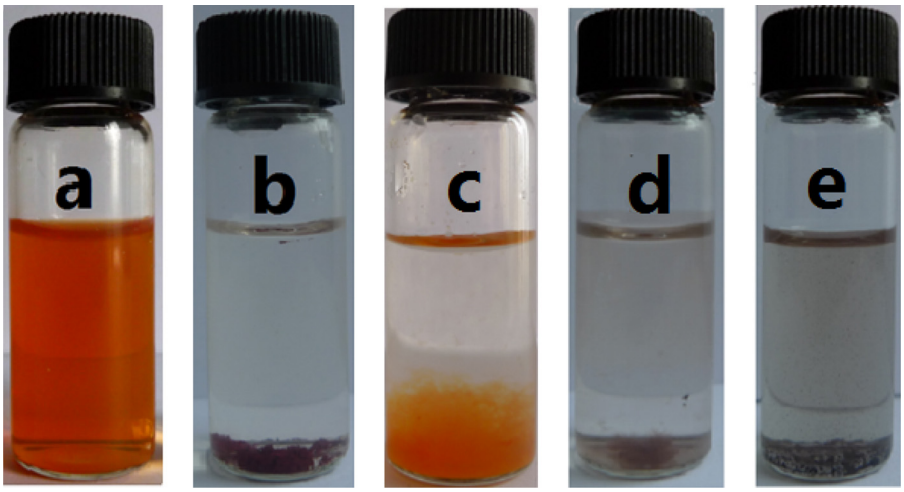

Fig. 2. Photographs of SeNPs in water in the presence (a) and absence (b) of s-LNT, (c) in the presence of t-LNT in the redox reaction after storage for 3 days. (d) and (e) The pictures of SeNPs in water after adding NaOH and DMSO into Se/s-LNT dispersion, respectively.

demonstrated that SeNPs were successfully prepared in the s-LNT aqueous solution.

3.2. Dispersion of SeNPs in the aqueous medium by s-LNT

As we know, the particles of elemental Se (Se^0) formed from the redox system of selenite and ascorbic acid or other reducing agents are unstable and can further aggregate into gray or black elemental Se if there was not any stabilizer, and the brick-red particles will be precipitated at the bottom of the cuvette. In the present work, the SeNPs with a weight-average diameter of ca. 28 nm were seen to be well dispersed in aqueous solution. As described in the Experimental, t-LNT after denaturation into s-LNT was added into the mixture of sodium selentie and ascorbic acid. To clarify the necessity of s-LNT in this system, dispersion of SeNPs by the carbohydrates including s-LNT and t-LNT was observed as shown in Fig. 2. It can be seen that the orange-red solution is still transparent without any precipitates in the presence of s-LNT (Fig. 2a), while the SeNPs aggregated into brownish black clusters and precipitated at the bottom of the vial resulting in the colorless supernatant in the absence of s-LNT (Fig. 2b). When adding t-LNT instead of s-LNT in the redox system, the orange-red SeNPs formed, but would not be completely dispersed into water and precipitate at the bottom of the vial after 3 d-storage (Fig. 2c), implying that the dispersion of SeNPs was not dependent on the high viscosity of polysaccharide because t-LNT has much higher viscosity than s-LNT. Obviously, s-LNT played an important role in the dispersion of SeNPs, which was further confirmed by adding NaOH and DMSO into Se/s-LNT dispersions. NaOH and DMSO are solvents with strong polarity, which can break the hydrogen bonding and Van der Waals's interaction. As shown in Fig. 2d and e, the SeNPs formed black aggregates and precipitated out within several hours after adding DMSO or NaOH into the Se/s-LNT solution. We thus could speculate that s-LNT chains interacted with SeNPs to form Se/s-LNT composites through hydrogen-bonding or Van der Waals's interaction.

To confirm this speculation, the Se/s-LNT composites were characterized by IR, and UV/vis as follows. As shown in Fig. 3A, t-LNT and Se/s-LNT had very similar spectra, and the characteristic absorption peak of hydroxyl group (OH) of t-LNT (3416 cm^{-1}) shift to a lower wave number of 3388 cm^{-1} for Se/s-LNT, indicating the hydrogen bonding interaction between the OH groups on the LNT chain and SeNPs. The results suggested that the LNT with the large number of hydroxyl groups could band to SeNPs through hydrogen bond-like interaction (Se—O—H) to avoid the aggregation of SeNPs. When DMSO or NaOH was added, the interaction of Se—O—H was disrupted, and SeNPs aggregated together resulting in precipitation as shown in Fig. 2d and e. Fig. 3B shows the UV/vis absorption of SeNPs, t-LNT, Se/s-LNT and Se/t-LNT dispersions or solutions at room temperature. Clearly, Se/s-LNT and Se/t-LNT show different UV/vis spectra from those of LNT and SeNPs, indicating interaction between SeNPs and LNT occurred. All the results from IR and UV/vis demonstrated the formation of Se/LNT composites in the presence of s-LNT.

In our previous published work (Jia et al., 2013), we have reported that s-LNT can renatured into triple helix with a hydrophobic cavity at concentration higher than 0.4 mg/mL. Gold

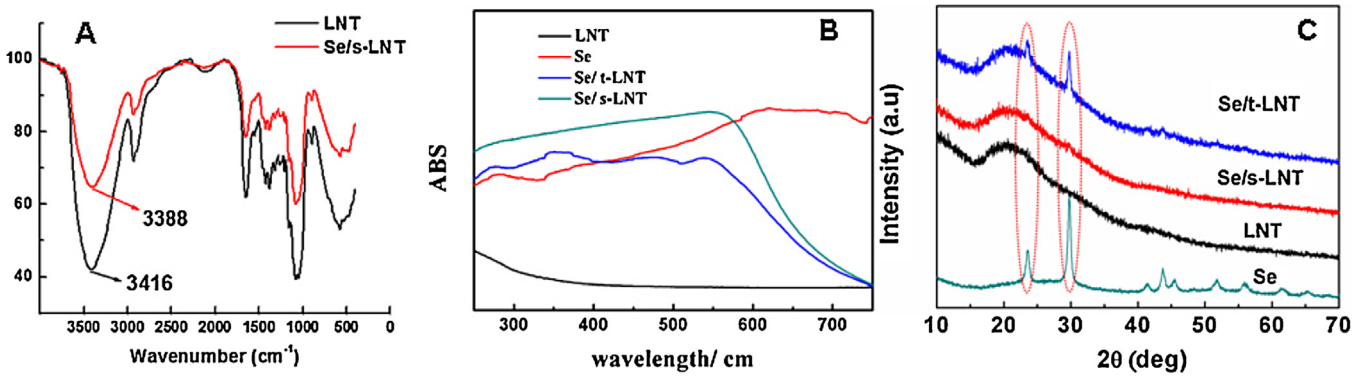

Fig. 3. The FT-IR spectra of t-LNT and Se/s-LNT(A), UV/vis spectra (B) and XRD pattern (C) of Se, LNT, Se/s-LNT and Se/t-LNT.

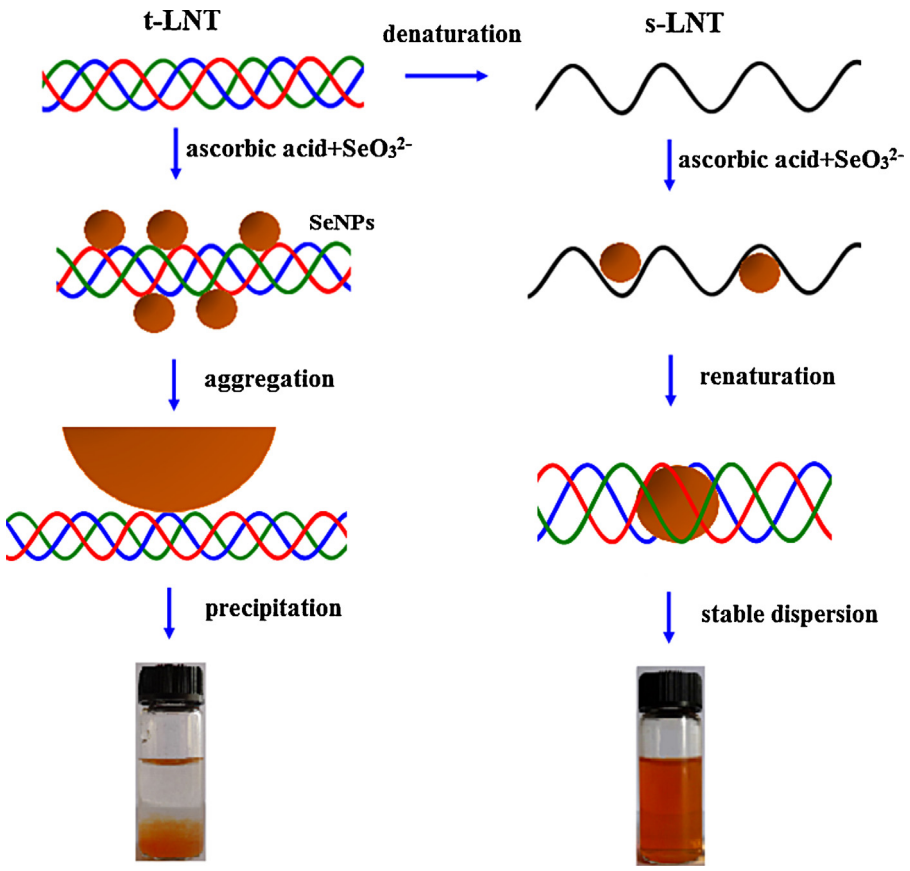

Fig. 4. Scheme of SeNPs dispersion by s-LNT and t-LNT.

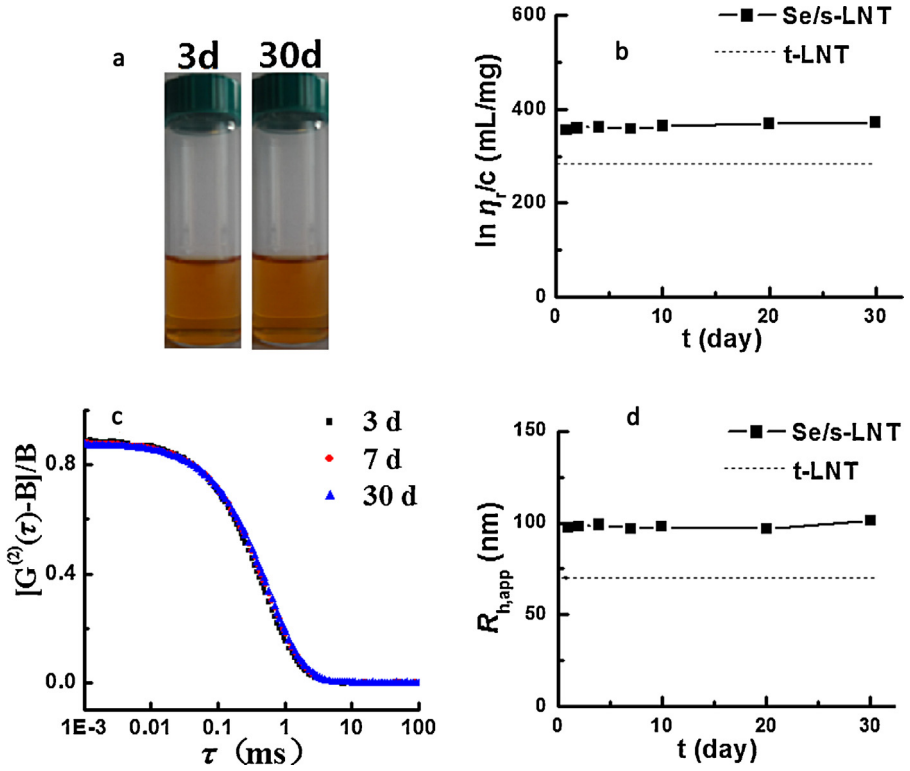

Fig. 5. (a) Solution color of Se/s-LNT aqueous solution (2 mg/mL) at room temperature for 3 and 30 days. (b) Time dependences of the apparent hydrodynamic radius ($R_{h,app}$) and intrinsic viscosity ([η]) for the Se/s-LNT aqueous solution at a fixed concentration of 2 mg/mL and 25 °C. (c) and (d) Intensity–intensity time correlation functions [$G^{(2)}(\tau)$] and the corresponding hydrodynamic radius distributions [$f(R_h)$] of the Se/s-LNT aqueous solution (2 mg/mL) with increasing storage time at $\theta = 90°$ and $T = 25$ °C.

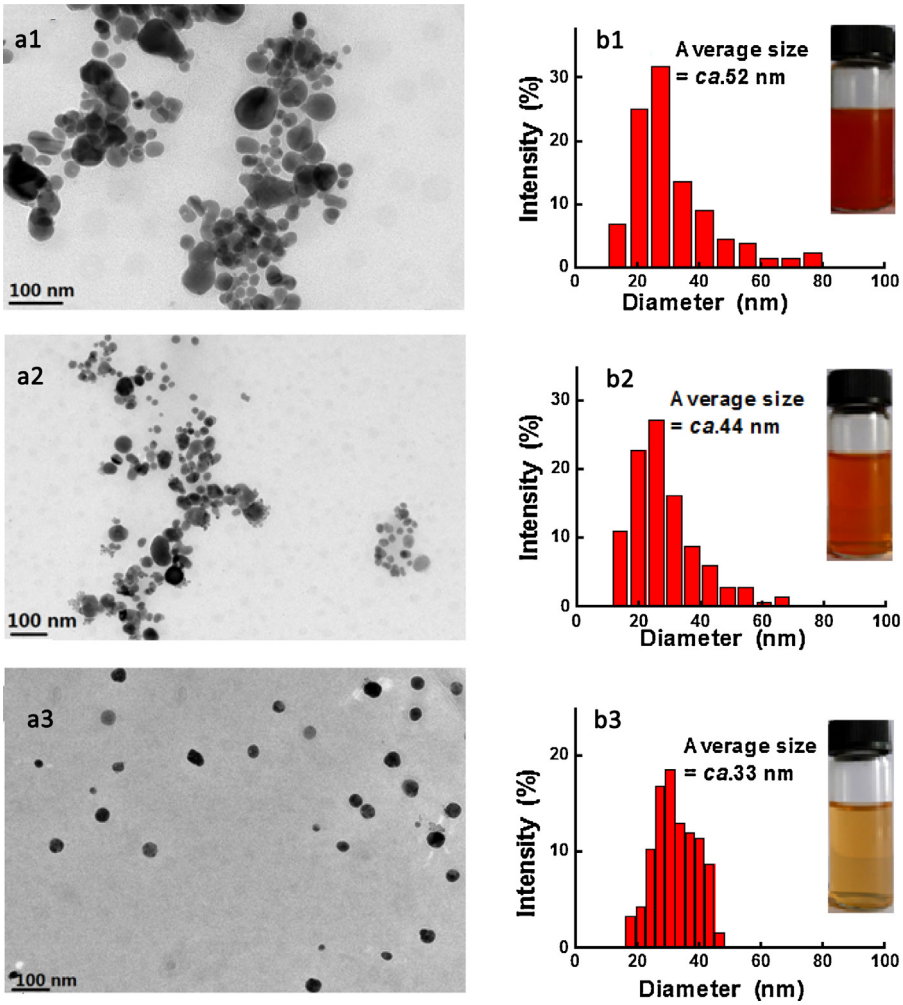

Fig. 6. TEM images (a1–3) and size distribution (b1–3) of selenium nanoparticles in Se/s-LNT-1, Se/s-LNT-2 and Se/s-LNT-3 aqueous solution (the reaction time was 3 days).

nanoparticles (AuNPs) can be entrapped into the cavity of the renatured LNT to form stable aqueous solution through hydrophobic interaction as the major driving force (Jia et al., 2013). As for silver nanoparticles (AgNPs), they are dispersed by t-LNT but not by s-LNT through AgNPs–O—H interaction. Once the t-LNT was broken by NaOH, the AgNPs aggregated into big clusters (Li et al., 2011a). The completely different dispersion mechanism is determined by the properties of the metal nanoparticles. AuNPs has stronger hydrophobicity than AgNPs, leading to difficult dispersion by t-LNT. Therefore, t-LNT was firstly broken into s-LNT, and AuNPs were entrapped into the hydrophobic cavity during the renaturation into triple helix. In this work the s-LNT concentration was near 2 mg/mL much higher than 0.4 mg/mL, and the renaturation will thus occur to form the ordered triple helix within ~4 h (Liu et al., 2012). According to the above results, we deduced the mechanism of SeNPs dispersion by s-LNT but not by t-LNT similar to AuNPs. Namely, SeNPs after synthesis were entrapped into the hydrophicity of the renatured triple helix. To confirm this dispersion of SeNPs by s-LNT, XRD experiments were performed. Fig. 3C shows a typical XRD pattern of the four samples including Se, LNT, Se/s-LNT and Se/t-LNT. All the reflection peaks of Se are similar to those reported in the literature (An, Tang, Liu, & Qian, 2003) demonstrated that the pure Se is successfully produced from this redox system. The strong and sharp reflection peaks at 2θ of 24° and 30° corresponded to the lattice planes of 100 and 101, respectively. After addition of t-LNT into the redox system, the two strong reflection peaks of 100 and 101 still occurred, suggesting the presence of the crystallic Se. However, the two typical peaks completely disappeared in the presence of s-LNT and showed the same pattern as that of the amorphous t-LNT, confirming the SeNPs were coated by the triple helix reformed by s-LNT, leading to the occurrence of amorphous SeNPs. Based on all the results described above, the schematic mechanism of dispersion of SeNPs by LNT was thus proposed as shown in Fig. 4.

3.3. Stability of the Se/s-LNT nanocomposites

The stability of the Se/s-LNT nanocomposites in the aqueous solution was investigated by DLS measurements and viscometry. The Se/s-LNT solution obtained by redissolving the as-prepared product of Se/s-LNT into water described in the experimental could remain homogeneous and translucent for 30 days (Fig. 5a), indicative of excellent stability. Fig. 5b shows the time dependence of the reduced viscosity ($\ln \eta_r/c$) of Se/s-LNT in water at 25 °C, along with the value of t-LNT. As a result, the $\ln \eta_r/c$ values in water hardly changed with increasing the storage time, revealing a strong stability because viscosity of the polymer in a solvent is an indication of molecular size and polymer chain extension of important parameters. Additionally, the $\ln \eta_r/c$ values of Se/s-LNT were higher than that of the original t-LNT, suggesting a larger size of Se/s-LNT than t-LNT. Fig. 5c shows the scattering light intensity–intensity correlation function $[G^{(2)}(\tau)]$ of Se/s-LNT in aqueous solution. It exhibited single exponential decay and only one relaxation mode with the same relaxation time. Namely, the correlation functions at different storage time indeed overlapped with each other, showing no

significant dependence on the standing time. It indicated that the observed mode of the scattering objects in the solution unchanged and the Se/s-LNT aqueous solution was a stable homogeneous system. By the Stokes–Einstein equation, the apparent hydrodynamic radius $R_{h,app}$ can be calculated (Fig. 5d). As a result, the $R_{h,app}$ of Se/s-LNT maintained at ca. 100 nm at scattering angle of 90° and hardly changed with time. Moreover, the $R_{h,app}$ of Se/s-LNT was a little higher than that of the original t-LNT, indicating formation of composite of Se/s-LNT, leading to the increase of the size. It was consistent with the viscosity result that the $\ln \eta_r/c$ values of Se/s-LNT were higher than that of the original t-LNT. All the above results demonstrated that SeNPs were well stabilized by s-LNT by forming nanocompite of Se/s-LNT.

In view of the above findings, we provided a method of dispersing and stabilizing SeNPs. When Na_2SeO_3 was dispersed in the s-LNT aqueous solution, it was reduced by ascorbic acid to generate element Se and the atoms would aggregate into SeNPs. As the hydroxyl groups of the s-LNT bind to the selenium atoms and the s-LNT renatured into a triple helical chain, Se/s-LNT nanocomposites was generated protecting SeNPs from further accumulation. Furthermore, the different size of SeNPs can be easily controlled by adjusting the oxidation–reduction reaction rate or the concentration of s-LNT.

3.4. SeNPs with different particle size distribution

Three samples of Se/s-LNT-1, Se/s-LNT-2, and Se/s-LNT-3 were prepared as described in the experimental section. According to the amount of added sodium selenite, we could calculate the final mass ratio of s-LNT and Se in three kinds of nanocomplexes Se/s-LNT-1, Se/s-LNT-2 and Se/s-LNT-3 is 5:1, 10:1 and 25:1, respectively. Fig. 6 shows the TEM images and size distribution (200 nanoparticles) of three complexes in aqueous solution. It can be seen as an increase in the proportion of s-LNT, the average size of the SeNPs decreased and the size distribution narrowed. Lin et al. proved that an increases of nano-selenium particle size will lead to the color change from light yellow to dark reddish brown. The inset images indicated the change of color for SeNPs. Thus we have successfully prepared three nano-selenium particles with different sizes.

In the two cases, SeNPs formation and renaturation of s-LNT occurred at the same time. The more is the Se content, is the redox reaction speed higher. Se/s-LNT-1 changed into red-brown after 10 min reaction, and Se/s-LNT-2 turned yellow in half an hour and gradually deepened. As analyzed above, SeNPs formed were entrapped into the reformed helical cavity of s-LNT. As the redox reaction speed was fast, the resulting SeNPs would have not enough time to enter into the renatured triple cavity, leading to aggregation of small SeNPs into large ones with broad size distribution as shown in Fig. 6a. With decreasing content of Se, more SeNPs could be wrapped by s-LNT, leading to smaller SeNPs dispersion with relatively narrow distribution. The little higher $R_{h,app}$ of Se/s-LNT than that of the original t-LNT implied that reformation of t-LNT and complexation between SeNPs and s-LNT, and the much better dispersion of Se/s-LNT than Se/t-LNT revealed that SeNPs entered into the reformed helical cavity of s-LNT.

The zeta potential of the three complexes was shown in Fig. 7. All the complexes showed the negative zeta potential, and Se/s-LNT-3 has the largest negative zeta potential in contrast to the other two complexes, indicating that Se/s-LNT-3 was more stable in aqueous solution. As is well known, the positive charges in the surfaces of complexes are essential for transfection into the cell because of the negative charges on the surfaces of cells. However, it has been reported in our previous work that s-LNT used as a gene carrier and the gene delivery system with negative zeta potentials could also be transfected into macrophages with high transfection efficiency (Liu et al., 2013). Negative zeta potential was also found to

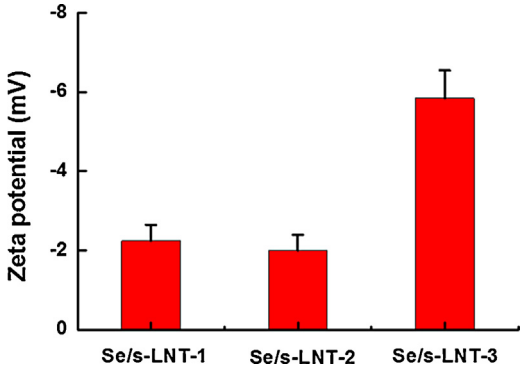

Fig. 7. Zeta potentials of Se/s-LNT-1, Se/s-LNT-2 and Se/s-LNT-3 in aqueous solution with concentration of 1.0 mg/mL at 25 °C.

be favorable for the nanoparticles uptake in the A549 cells (Patil, Sandberg, Heckert, Self, & Seal, 2007). So, the positive zeta potential of Se/s-LNT complexes is not the essential factor.

3.5. Antitumor activity of Se/s-LNT

The anti-tumor activity of the Se/s-LNT with different size distribution was tested by Hela cells using MTT assay described in the experimental part. Fig. 8 shows the effect of particle size on the apoptosis of Hela cells. It is clear that, with increasing concentration of s-LNT basically did not show the inhibition of Hela cells, which can be considered as s-LNT in the complex Se/s-LNT only play the role of dispersing SeNPs, not on the antitumor activity in vitro. Without the protection of s-LNT, selenium nanoparticles gathered and settled in the cell culture, leading to a lower bioactivity and cause it did not show antitumor activity in vitro. The half inhibitory concentrations (IC_{50}), which was defined as the Se concentration in the complex at which half of the cells growth are inhibited, of three complexes Se/s-LNT-1, Se/s-LNT-2, Se/s-LNT-3 were estimated to be 85, 37, and 19 μM. That is, with decreasing size and size distribution of SeNPs, the antitumor activity increased, indicating that the aggregated SeNPs with large size had lower ability to kill tumor cells. Taken together, SeNPs with small uniform size largely enhanced the antitumor activity and bioavailability.

3.6. ROS generation

Reactive oxygen species (ROS) are chemically reactive molecules containing oxygen such as superoxide anion, hydroxyl, peroxyl, and alkoxyl radicals. Cancer cells exhibit greater ROS stress than normal cells do, partly due to that the anti-oxidant capability of normal cells is stronger than that of the tumor cells (Zhang et al., 2013). ROS is a double-edged sword. On one hand, at low levels, ROS facilitates cancer cell survival since cell-cycle progression driven by growth factors and receptor tyrosine kinases (RTK) require ROS for activation and chronic inflammation (Irani, 1997). On the other hand, high levels of ROS could cause cellular damage depending on the duration of ROS stress to mediate apoptosis by regulating the expression of various apoptosis regulatory proteins, and could therefore function as anti-tumor growth through the sustained activation of cell-cycle inhibitor and induction of cell death as well as senescence by damaging macromolecules (Ramsey & Sharpless, 2006). In fact, a lot of the chemotherapeutic and radio-therapeutic agents kill cancer cells by increasing ROS stress. So there is a novel therapy for anti-cancer that preferentially eradicates cancer cells by targeting the ROS stress response pathway. ROS generation also acted as an important role in Se compounds, especially in SeNPs-induced cancer cell apoptosis. As shown in Fig. 8c, the mean fluorescence intensity of

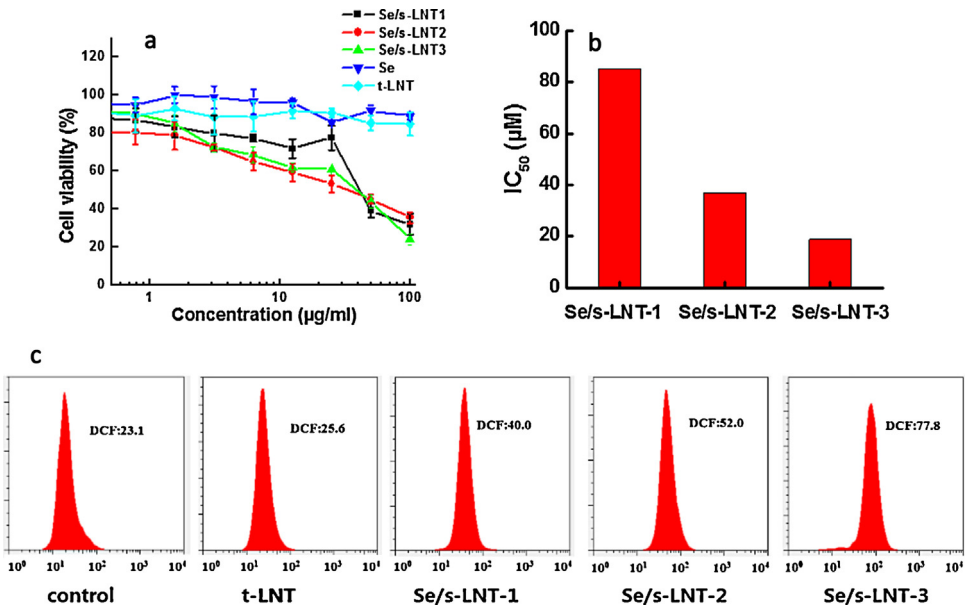

Fig. 8. Effects of Se, t-LNT and Se/s-LNT-1,2,3 on the growth of Hela cells (a), values expressed are means ± SD of three replicates. (b) IC_{50} of SeNPs in different composites of Se/s-LNTs. 1, 2 and 3 denoted by the different mass ratios of s-LNT and Se as 5:1, 10:1, and 25:1, respectively. (c) Flow cytometric analysis of ROS levels in Hela cells treated by different complexes Se/s-LNT. Hela cells were treated with t-LNT (200 μg/mL) and 2.0 μg of Se included in different composites of Se/s-LNT-1 (12 μg/mL), Se/s-LNT-2 (22 μg/mL) and Se/s-LNT-3 (52 μg/mL).

Se/s-LNT treated cells ranged from 40.0 to 78.8 with decreasing the size of SeNPs, much higher than that of control group (23.1) and t-LNT-treated group (25.6), showing the potential role of ROS in Se/s-LNT induced HeLa cell apoptosis. Additionally, SeNPs with the same content of 2.0 μg in the complex but different particle size showed different ability of ROS generation. The smaller is the size of SeNPs, the higher is the ROS production. The increasing ROS induced by Se/s-LNT demonstrated that SeNPs could disturb the balance of ROS in Hela cells to induce cell death as shown in Fig. 8a.

4. Conclusions

In this work, we discovered a new approach for dispersion and stabilization of SeNPs in aqueous medium. SeNPs was successfully synthesized from Se^{4+} by the acid and dispersed using the single chain (s-LNT) of a triple helical β-glucan coded as t-LNT. It was proved that hydroxyl groups of LNT interacted with SeNPs contributing to the dispersion of SeNPs in water. Especially, the coating of SeNPs by the hydrophobic cavity of the renatured triplex from s-LNT contributed to the stable dispersion of SeNPs in water. We also successfully synthesized SeNPs with different size by adjusting the oxidation–reduction reaction rate or the content of s-LNT. In-vitro experiments indicated that the SeNPs with smaller size could be distributed uniformly in complexes and showed higher anti-tumor activity. Lentinan basically did not show the inhibition of Hela cells in vitro, which can be considered that lentinan in the complex Se/s-LNT only played the role of dispersing SeNPs.

Acknowledgements

We gratefully acknowledge the financial supports from the National Natural Science Foundation of China (21274114 and 20874078), New Century Excellent Talents Program of Education Ministry (NCET-13-0442), Yellow Crane Talent Program of Wuhan City (2012), and National Basic Research Program of China (973 Program, 2010CB732203).

References

An, C., Tang, K., Liu, X., & Qian, Y. (2003). Large-scale synthesis of high quality trigonal selenium nanowires. *European Journal of Inorganic Chemistry*, *0*(17), 3250–3255.
Bao, Y., & Williamson, G. (2000). Selenium-dependent glutathione peroxidases. *Progress in Natural Science*, *10*, 321–330.
Brown, K., & Arthur, J. (2001). Selenium, selenoproteins and human health: A review. *Public Health Nutrition*, *4*(2B SPI), 593–600.
Chen, T., Wong, Y.-S., Zheng, W., Bai, Y., & Huang, L. (2008). Selenium nanoparticles fabricated in *Undaria pinnatifida* polysaccharide solutions induce mitochondria-mediated apoptosis in A375 human melanoma cells. *Colloids and Surfaces B: Biointerfaces*, *67*(1), 26–31.
Cho, D. Y., Jung, U., & Chung, A. S. (1999). Induction of apoptosis by selenite and selenodiglutathione in HL-60 cells: Correlation with cytotoxicity. *IUBMB Life*, *47*(5), 781–793.
Clark, L. C., Combs, G. F., Turnbull, B. W., Slate, E. H., Chalker, D. K., Chow, J., et al. (1996). Effects of selenium supplementation for cancer prevention in patients with carcinoma of the skina randomized controlled trial. *JAMA: The Journal of the American Medical Association*, *276*(24), 1957–1963.
Fang, W., Han, A., Bi, X., Xiong, B., & Yang, W. (2010). Tumor inhibition by sodium selenite is associated with activation of c-Jun NH_2-terminal kinase 1 and suppression of β-catenin signaling. *International Journal of Cancer*, *127*(1), 32–42.
Huang, B., Zhang, J., Hou, J., & Chen, C. (2003). Free radical scavenging efficiency of nano-Se in vitro. *Free Radical Biology and Medicine*, *35*(7), 805–813.
Irani, K. (1997). Mitogenic signaling mediated by oxidants in ras-transformed fibroblasts. *Science*, *275*(5306), 1649–1652.
Jia, X., Xu, X., & Zhang, L. (2013). Synthesis and stabilization of gold nanoparticles induced by denaturation and renaturation of triple helical β-glucan in water. *Biomacromolecules*, *14*(6), 1787–1795.
Kashiwada, S. (2006). Distribution of nanoparticles in the see-through medaka (*Oryzias latipes*). *Environmental Health Perspectives*, *114*(11), 1697–1702.
Li, Q., Chen, T., Yang, F., Liu, J., & Zheng, W. (2010). Facile and controllable one-step fabrication of selenium nanoparticles assisted by L-cysteine. *Materials Letters*, *64*(5), 614–617.
Li, S., Zhang, Y., Xu, X., & Zhang, L. (2011). Triple helical polysaccharide-induced good dispersion of silver nanoparticles in water. *Biomacromolecules*, *12*(8), 2864–2871.
Li, Y., Li, X., Wong, Y.-S., Chen, T., Zhang, H., Liu, C., et al. (2011). The reversal of cisplatin-induced nephrotoxicity by selenium nanoparticles functionalized with 11-mercapto-1-undecanol by inhibition of ROS-mediated apoptosis. *Biomaterials*, *32*(34), 9068–9076.
Lin, Z.-H., & Chris Wang, C. R. (2005). Evidence on the size-dependent absorption spectral evolution of selenium nanoparticles. *Materials Chemistry and Physics*, *92*(2–3), 591–594.
Liu, Q., Wang, C., Cao, Y., Xu, X., & Zhang, L. (2013). A novel gene carrier prepared from triple helical β-glucan and polydeoxyadenylic acid. *Journal of Materials Chemistry B*, *2*(8), 933–944.
Liu, Q., Xu, X., & Zhang, L. (2012). Variable chain conformations of renatured β-glucan in dimethylsulfoxide/water mixture. *Biopolymers*, *97*(12), 988–997.

Lu, Q., Gao, F., & Komarneni, S. (2006). Cellulose-directed growth of selenium nanobelts in solution. *Chemistry of Materials*, *18*(1), 159–163.
Menter, D. G., Sabichi, A. L., & Lippman, S. M. (2000). Selenium effects on prostate cell growth. *Cancer Epidemiology Biomarkers & Prevention*, *9*(11), 1171–1182.
Patil, S., Sandberg, A., Heckert, E., Self, W., & Seal, S. (2007). Protein adsorption and cellular uptake of cerium oxide nanoparticles as a function of zeta potential. *Biomaterials*, *28*(31), 4600–4607.
Peng, D., Zhang, J., Liu, Q., & Taylor, E. W. (2007). Size effect of elemental selenium nanoparticles (nano-Se) at supranutritional levels on selenium accumulation and glutathione *S*-transferase activity. *Journal of Inorganic Biochemistry*, *101*(10), 1457–1463.
Pi, J., Jin, H., Liu, R., Song, B., Wu, Q., Liu, L., et al. (2013). Pathway of cytotoxicity induced by folic acid modified selenium nanoparticles in MCF-7 cells. *Applied Microbiology and Biotechnology*, *97*(3), 1051–1062.
Ramamurthy, C. H., Sampath, K. S., Arunkumar, P., Kumar, M. S., Sujatha, V., Premkumar, K., et al. (2013). Green synthesis and characterization of selenium nanoparticles and its augmented cytotoxicity with doxorubicin on cancer cells. *Bioprocess and Biosystems Engineering*, *36*(8), 1131–1139.
Ramsey, M. R., & Sharpless, N. E. (2006). ROS as a tumour suppressor? *Nature Cell Biology*, *8*(11), 1213–1215.
Sasaki, T., & Takasuka, N. (1976). Further study of the structure of lentinan, an anti-tumor polysaccharide from *Lentinus edodes*. *Carbohydrate Research*, *47*(1), 99–104.
Shen, Y., Wang, X., Xie, A., Huang, L., Zhu, J., & Chen, L. (2008). Synthesis of dextran/Se nanocomposites for nanomedicine application. *Materials Chemistry and Physics*, *109*(2–3), 534–540.
Wang, D., Guo, Z., Ma, X., Hu, Y., Huang, X., Fan, Y., et al. (2010). Effects of sulfated lentinan on cellular infectivity of avian infectious bronchitis virus. *Carbohydrate Polymers*, *79*(2), 461–465.
Wang, H., Zhang, J., & Yu, H. (2007). Elemental selenium at nano size possesses lower toxicity without compromising the fundamental effect on selenoenzymes: Comparison with selenomethionine in mice. *Free Radical Biology and Medicine*, *42*(10), 1524–1533.
Wang, X., Xu, X., & Zhang, L. (2008). Thermally induced conformation transition of triple-helical lentinan in NaCl aqueous solution. *The Journal of Physical Chemistry B*, *112*(33), 10343–10351.
Wang, X., Zhang, X., Xu, X., & Zhang, L. (2012). The LiCl effect on the conformation of lentinan in DMSO. *Biopolymers*, *97*(10), 840–845.
Xu, X., Chen, P., Zhang, L., & Ashida, H. (2012). Chain structures of glucans from *Lentinus edodes* and their effects on NO production from RAW 264.7 macrophages. *Carbohydrate Polymers*, *87*(2), 1855–1862.
Xu, X., Pan, C., Zhang, L., & Ashida, H. (2011). Immunomodulatory β-glucan from *Lentinus edodes* activates mitogen-activated protein kinases and nuclear factor-κB in murine RAW 264.7 macrophages. *Journal of Biological Chemistry*, *286*(36), 31194–31198.
Xu, X., Wang, X., Cai, F., & Zhang, L. (2010). Renaturation of triple helical polysaccharide lentinan in water-diluted dimethylsulfoxide solution. *Carbohydrate Research*, *345*(3), 419–424.
Xu, X., Yasuda, M., Nakamura-Tsuruta, S., Mizuno, M., & Ashida, H. (2012). β-Glucan from *Lentinus edodes* inhibits nitric oxide and tumor necrosis factor-α production and phosphorylation of mitogen-activated protein kinases in lipopolysaccharide-stimulated murine RAW 264.7 macrophages. *Journal of Biological Chemistry*, *287*(2), 871–878.
Zhang, J., Gao, X., Zhang, L., & Bao, Y. (2001). Biological effects of a nano red elemental selenium. *Biofactors*, *15*(1), 27–38.
Zhang, J., Wang, H., Bao, Y., & Zhang, L. (2004). Nano red elemental selenium has no size effect in the induction of seleno-enzymes in both cultured cells and mice. *Life Sciences*, *75*(2), 237–244.
Zhang, J., Wang, X., & Xu, T. (2008). Elemental selenium at nano size (nano-Se) as a potential chemopreventive agent with reduced risk of selenium toxicity: Comparison with Se-methylselenocysteine in mice. *Toxicological Sciences*, *101*(1), 22–31.
Zhang, L., Wang, L., Hu, Y., Liu, Z., Tian, Y., Wu, X., et al. (2013). Selective metabolic effects of gold nanorods on normal and cancer cells and their application in anticancer drug screening. *Biomaterials*, *34*(29), 7117–7126.
Zhang, L., Zhang, X., Zhou, Q., Zhang, P., Zhang, M., & Li, X. (2001). Triple helix of. BETA.-D-glucan from lentinus edodes in 0.5 M NaCl aqueous solution characterized by light scattering. *Polymer Journal*, *33*(4), 317–321.
Zhang, Y., Wang, J., & Zhang, L. (2010). Creation of highly stable selenium nanoparticles capped with hyperbranched polysaccharide in water. *Langmuir*, *26*(22), 17617–17623.